Optical design of the Orbiting Astronomical Satellite for Investigating Stellar Systems

Siddhartha Sirsi[a,b,*] **Yuzuru Takashima**[b] **Arthur Palisoc**[c] **Heejoo Choi**[b,d] **Jonathan W. Arenberg**[e] **Daewook Kim**[a,b,d] **and Chistopher Walker**[a,b]

[a]University of Arizona, Department of Astronomy and Steward Observatory, Tucson, Arizona, United States
[b]University of Arizona, Wyant College of Optical Sciences, Tucson, Arizona, United States
[c]L'Garde, Inc., Tustin, California, United States
[d]University of Arizona, Large Binocular Telescope Observatory, Tucson, Arizona, United States
[e]Northrop Grumman Systems Corporation, Redondo Beach, California, United States

Abstract. The Orbiting Astronomical Satellite for Investigating Stellar Systems (OASIS) is a proposed space telescope with a 14-m inflatable primary reflector that will perform high spectral resolution observations at terahertz frequencies with heterodyne receivers. The telescope consists of an inflatable metallized polymer membrane that serves as the primary antenna, followed by aberration correction optics, and a scanner that enables a 0.1-deg field of regards while achieving diffraction-limited performance over wavelength range from 63 to 660 μm. Here, the parametric solution space of the OASIS inflatable telescope design is systematically investigated by establishing analytical relations among figure of merits including first-order geometrical photon collection area and the size of correction optics. The first-order solution was further optimized by ray-trace code by incorporating numerically calculated mirror shape with preformed membrane gores. Design study shows that a space-based telescope with an effective photon collection area of over 90 m^2 can be achieved by utilizing a 14-m inflatable aperture.
 [DOI: 10.1117/1.JATIS.8.3.034002]

Keywords: Orbiting Astronomical Satellite for Investigating Stellar Systems; terahertz astronomy; inflatable reflector; space telescope; optical design; scanner.

Paper 22034G received Mar. 9, 2022; accepted for publication Aug. 3, 2022; published online Aug. 16, 2022.

1 Introduction

Water is an essential ingredient in the origin and evolution of life on Earth.[1] Water also plays an important role in the formation of planets. The Orbiting Astronomical Satellite for Investigating Stellar Systems (OASIS) is a proposed space-based telescope with a 14-m-diameter inflatable primary reflector/antenna that will follow the water trail from galaxies to oceans by performing high spectral resolution observations of water at terahertz frequencies.[2,3] The telescope's primary reflector consists of transparent and metalized polymer membranes sealed around their periphery, constrained by a tensioning structure, and inflated to the required pressure (Fig. 1). The large inflatable primary antenna (A1) is the key to achieving the large collecting areas required for the proposed observational study. OASIS will have ~10× the collecting area and 6× the angular resolution of the Herschel Space Observatory[4] and compliments the short-wavelength capabilities of James Webb Space Telescope (0.6 to 28.3 μm). Such a large aperture is realized by utilizing a lightweight, stowable polymer-based primary antenna that reduces launch cost, as well as the lead time required for fabrication.

The shape of the primary antenna A1 is a function of pressure, material properties, and boundary conditions. The dependence of the shape of A1 on multiple parameters offers unique opportunities for achieving design goals. The shape of inflatable membranes has been discussed in

*Address all correspondence to Siddhartha Sirsi, ssirsi@email.arizona.edu

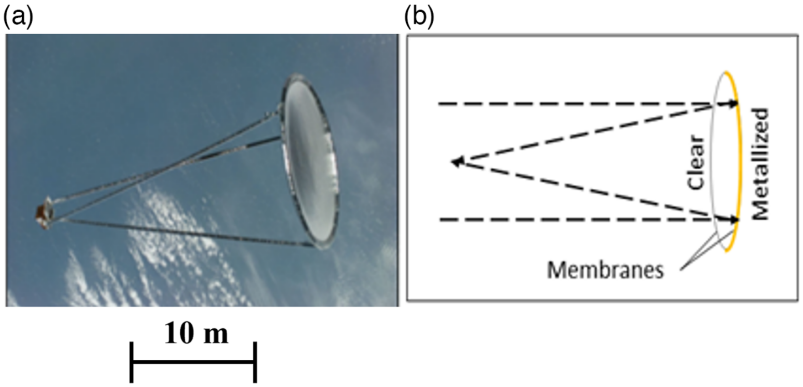

Fig. 1 (a) Inflatable aperture experiment (IAE) demonstrated a 14-m inflatable aperture in space (1996) for use at X-band. (b) Incoming signal focused by concave metallized membrane (Image: NASA).

several articles. A fourth-order solution for the uniformly loaded inflated monolithic membrane is reported by Hencky.[5] Surface shape with higher-order terms is presented by Fichter.[6] Besides these analytic solutions, the finite element analyzer for membranes (FAIM) software package was developed by L'Garde Inc. to numerically calculate the shape of A1 after inflation. This numerical approach was adopted to simulate the final inflated shape of A1 under different conditions.[7]

Inflated membrane reflectors formed from flat dielectric sheets inherently form Hencky surfaces. Hencky surfaces are neither spherical nor parabolic and involve coupled second- and fourth-order terms. In this situation, the magnitude of the spherical aberration in A1 is coupled to its focal length, $F/\#$. An approach for correcting spherical aberration and focus utilizing four mirrors is reported by Burge et al.[8] The OASIS' aberration correction mirror pair is designed to simultaneously tackle the on-axis spherical aberrations and off-axis aberrations, i.e., coma, encountered with an inflatable. Moreover, the effective collection area of the telescope and secondary mirror sizes are also a function of the shape and size of A1. In addition, the wide wavelength range of OASIS requires appropriate tolerance budgeting.

Within the complex and mutually coupled design landscape, we have developed a first-order analytical model for inflatable reflectors. Based on the first-order model, further optimization of corrector optics, as well as tolerance analysis is performed as a function of collecting area and effective focal length (EFL) ($F/\#$). This approach determines the optimal design that delivers the required effective collection area utilizing a compact aberration correcting mirror pair. The results are presented in the form of solution space contour plots, which serve as a powerful tool for converting scientific requirements to optical system specifications.

Here we report the design process of a large aperture telescope with an inflatable primary reflector. In Sec. 2 the OASIS optical specification is discussed in conjunction with the concept of operation. In Sec. 3, power arrangement, size requirement for correction optics, and photon collection area are addressed by developing an analytical model based on a fourth-order Hencky model. Further optimization of the corrector optics, incorporation of a numerical solution for surface shape, and a performance figure of merit is discussed in Sec. 4. Section 5 addresses photon collection area as a function of EFL and $F/\#$ of the primary mirror in the design space while incorporating additional factors influencing on photon collection area, e.g., as-built Strehl intensity ratio (SIR) and optical transmission. Section 6 discusses the optical design of a field of view (FoV) scanning mechanism for OASIS. The baseline design and optical path loss budget of a 14-m OASIS space telescope is discussed in Sec. 7, followed by a discussion of how to address challenges encountered in the design of inflatable optical systems.

2 OASIS Optical Specifications

The OASIS space telescope concept is illustrated in Fig. 2. Its 14-m primary reflector, A1, is initially stowed in the spacecraft and deployed in orbit using three expanding booms.[9] A1 is made up of two thin ($\sim$12 μm) polymer (e.g., Mylar or Kapton) membranes; one forming a

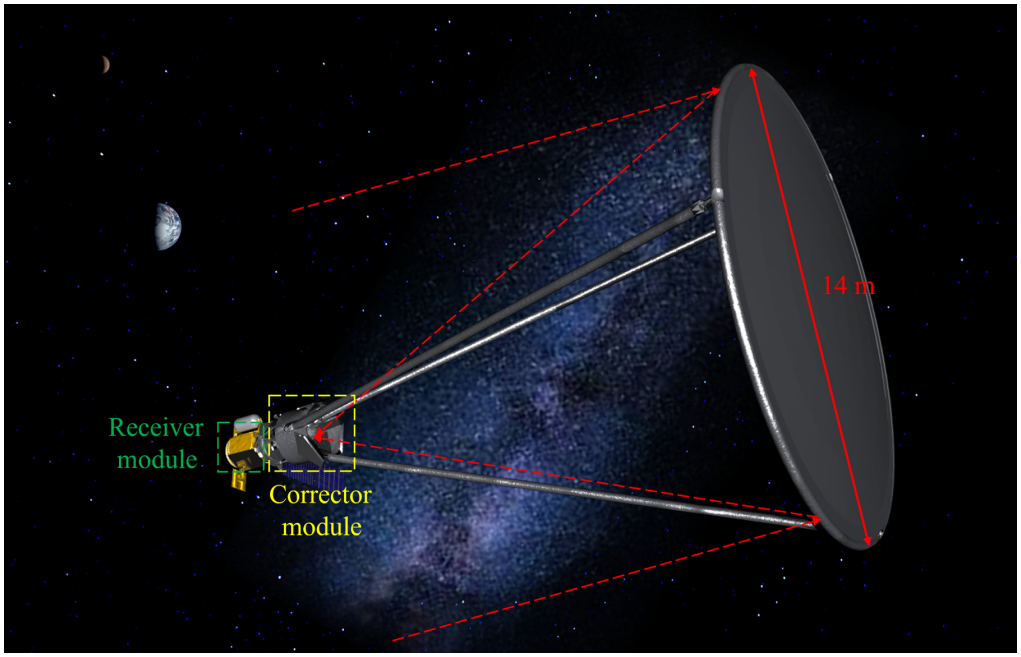

Fig. 2 OASIS mission concept showing the corrector and receiver modules (left side of the figure) and the fully deployed 14-m diameter primary reflective antenna A1 (right side of the figure), which is an inflatable membrane optic.

Table 1 Key optical design requirements of OASIS based on science goals and system architecture.

	Requirement
F/#	16
Collection area	>56 m^2
FoV	±3 arcmin (circle)
Payload mass/collection area	13 kg/m^2
Wavelength	63 to 660 μm

clear canopy and the second an aluminized reflector. The space between the two membranes is pressurized to form the required concave reflective surface.

OASIS targets far-infrared (far-IR) transitions of water and its isotopologues, as well as HD and other molecular species, from 0.45 to 4.7 THz (660 to 63 μm) that are obscured by the Earth's atmosphere. The sensitivity required to detect and spectrally resolve these lines is provided by a large aperture coupled with state-of-the-art heterodyne receivers.[10] The terahertz heterodyne receivers need to be periodically (~20 s) chopped on and off-targets. This translates to a minimum required FoV of 0.01 deg (6 arcmin). An $F/16$ system is selected to efficiently couple the telescope beam to the focal plane instruments. The key requirements concerning the optical design of OASIS are listed in Table 1.

3 Analytical Model of A1 with Spherical Aberration Corrector

3.1 *Shape of Inflatable Primary Antenna A1*

An inflatable mirror formed by pressurizing two thin, circular, monolithic flat polymer membranes bonded at the edges has a surface profile of an oblate spheroid whose figure can be expressed by an even power series known as Hencky curve,[11] given as

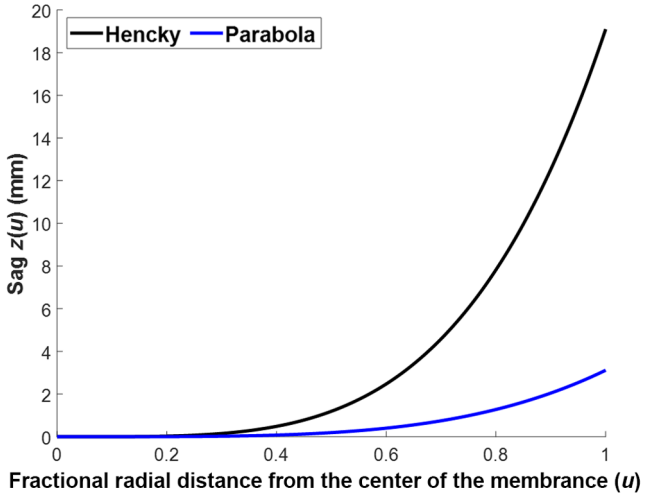

Fig. 3 Comparison between Hencky and parabolic surface radial profile with the best fit sphere removed.

$$z(u) = \frac{D}{64F^2}(u^2 + 0.1111u^4), \tag{1}$$

where D is the diameter of the mirror, F is the $F/\#$, and $u = \frac{r}{D}$ is the fractional radius. A Hencky surface will be assumed for A1 in the first-order optical design.

Figure 3 plots $z(u)$ for a Hencky surface with $D = 20$ m, and $F = 1.25$. For the purpose of comparison, parabolic sag for the same D and $F/\#$ is also shown. Because the sag value at the edge of mirror substantially deviates from the sag of parabola, a large amount of spherical aberration is induced by the Hencky surface.

3.2 *First-Order OASIS Optical Design Layout*

To correct for the spherical aberration due to the deviation of A1 from an ideal parabola, two concave mirrors, M2 and M3, are incorporated in the optical design as shown in Fig. 4. This mirror pair resides in the corrector module (Fig. 2). Together they correct for both spherical

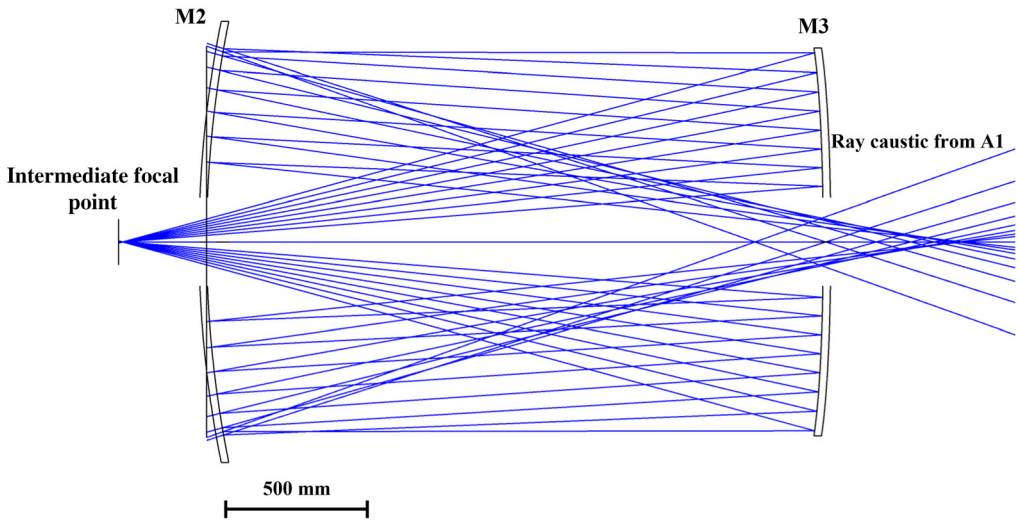

Fig. 4 Optical layout of OASIS corrector M2-M3 mirror pair. Signal from the astronomical target reflects off A1, passes through M3 hole, reflects off M2, and is re-imaged by M3 through the M2 center hole.

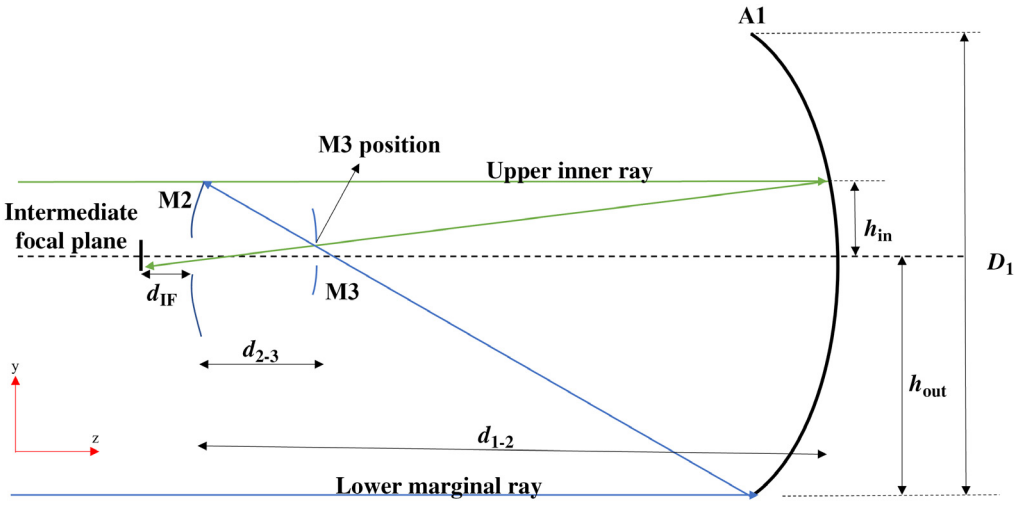

Fig. 5 Analytical model showing the ray trace used to determine the systematic design space set by the mirror positions and critical dimensions of the corrector optics pair (M2 and M3).

aberration and off-axis aberrations (e.g., coma). The driving principles behind the design of the M2 and M3 mirror pair are to

i. achieve the smallest possible mirror size,
ii. minimize the distance between mirror pairs while also minimizing the central hole diameter of the M2 and M3 mirrors, and
iii. maximize the geometrical photon collection area.

To satisfy those requirements, we adopted a power arrangement of the A1–M2–M3 system that is similar to that of a reflective null collector.[12] The M2 mirror is placed at the paraxial focus of A1 and corrects for the spherical aberration induced by A1. M3 relays paraxial focus of A1 back to M2, which is also the system focal point of A1–M2–M3. In this sense, M3 is a 1:1 relay optics that reimages the intermediate image formed by A1 to the location of M2 again while jointly correcting spherical aberration with M2. To maximize the effective collection area, the diameter of the central hole of M2 and M3 mirrors are minimized by placing M3 where the size of ray bundle of A1 is minimized or at the minimum blur position.[13]

As depicted in Fig. 5, diameter (D_1) and focal length of A1 (or distance between A1 and M2: d_{1-2}) are chosen as primary design variables, since those determine the overall dimensions of the A1–M2–M3 optical system, which is constrained by science/mission requirements for aperture size and stow volume. Given D_1, the surface profile of A1 and d_{1-2} is a function of pressure and membrane properties. For the parameters D_1 and d_{1-2}, viable M2–M3 corrector designs can be identified by using the approach described below.

3.3 *Design Space Survey Using Iterative Analytical Model*

The central obscuration of A1 (h_{in}) is dependent on M2, the M3 location, and the M3 entrance hole size. In turn, the location of M2 is dependent on the location of M3. An iterative analytical model was developed to optimize the first order power arrangement and solve or h_{in}, with its mutually coupled dependencies. This model determines the location and size of M2–M3 corrector optics, and the geometrical collection area of the telescope system by evaluating the value of h_{in} for different combinations of A1 surface profiles and apertures. The first-order design process is divided into substeps 1 through 7 as follows:

An iterative analytical model is run using the parameters in Table 2.

Step 1: The Hencky surface profile is obtained for a given D_1, d_{1-2}, and FoV (θ) with M2 hole diameter (H_{M2})

Table 2 Iterative analytical model parameters.

Model parameters	Value
R_1	50 m
D_1	[12 m, 13 m, 14 m, 15 m, 16 m, 17 m]
d_{2-3}	2.2 m
d_{IF}	200 mm
Θ	±0.05 deg

$$H_{M2} = 2\,\tan(\theta) d_{1-2} + \frac{d_{IF}}{(f/\#)_{\text{sys}}}, \tag{2}$$

where $(f/\#)_{\text{sys}}$ is system $F/\#$, d_{IF} is a distance from M2 mirror surface to focal plane of the A1-M2–M3 system, $d_{1-2} = \frac{R_1}{2}$, and R_1 is the base radius of curvature of A1. In Eq. (2), $d_{IF}/(f/\#)_{\text{sys}}$ is the ray bundle size at the surface of M2. The M2 hole size H_{M2} accommodates the ray bundle footprint, while taking into account the shift of the ray bundle by an amount $2\,\tan(\theta) d_{1-2}$.

Step 2: Calculate the height (h_{in}) of the incident ray (labeled as upper inner ray in Fig. 5) at A1, which results in an image height of $H_{M2}/2$ at the initial intermediate focal plane. $h_{\text{out}} = D_1/2$ is the height of the marginal ray at A1 (labeled as lower marginal ray in Fig. 5).

Step 3: The intersection of the upper inner ray and the lower marginal ray determines the location of M3 where the ray bundle size is minimized with spherical aberration of A1, as well as its hole size (H_{M3}).

Step 4: Given the distance d_{2-3} between M2 and M3, the location of M2 is updated.
Steps 1 to 4 are iterated until the value of h_{in} converges.

Step 5: The height of the lower marginal ray at the updated location of M2 determines the diameter of M2 (D_{M2}).

Step 6: Diameter of M3 (D_{M3}) is calculated by equating the $(f/\#)_{\text{sys}}$ with $(f/\#)_{M3}$ as

$$(f/\#)_{\text{sys}} = \frac{(R_1/2)}{2h_{\text{out}}}, \tag{3}$$

$$(f/\#)_{M3} = \frac{d_{2-3} + d_{\text{IF}}}{D_{M3}}, \tag{4}$$

$$D_{M3} = (d_{2-3} + d_{\text{IF}}) \frac{2h_{\text{out}}}{R_1/2}. \tag{5}$$

Step 7: Geometrical photon collection area (CA_{Geo}) of the system is calculated

$$\text{CA}_{\text{Geo}} = (h_{\text{out}}^2 - h_{\text{in}}^2)\pi. \tag{6}$$

The results of the parametric sweep of D_1 for $R_1 = 50$ m and its comparison with the results calculated by geometrical raytracing software (ZEMAX, CodeV) are listed in Table 3. The shape of the M2 and M3 mirrors is optimized to provide diffraction limited performance.

The geometrical photon collection area of A1 calculated by the analytical model is in close accordance with the ZEMAX model. Table 3 shows that the iterative analytical model can be used to accurately predict the optical design parameters without having to go through the entire design process using ray tracing software. One important finding from the first-order analysis is that Hencky surface profile of A1 requires M2 and M3 diameters exceeding 1 m.

Table 3 Comparison of parametric sweep of D_1 for $R_1 = 50$ m between the analytical and ray tracing software (ZEMAX models).

D_1 (m)	d_{1-2} (m)	D_{M2} (m)	H_{M2} (mm)	D_{M3} (m)	H_{M3} (mm)	Analytical geometrical photon collection area (m^2)	Geometrical photon collection area by ZEMAX (m^2)
12	25.7705	1.33	141	1.15	134	102.55	100.31
13	25.5295	1.52	149	1.24	208	116.62	116.3
14	25.2675	1.74	156	1.34	301	129.62	129.21
15	24.9872	1.97	164	1.44	410	141.49	140.91
16	24.6881	2.23	171	1.53	533	152.29	151.72
17	24.3737	2.51	179	1.63	665	162.61	161.67

Note: D_1, Entrance pupil diameter of A1; d_{1-2}, Distance between A1 and M2; D_{M2}, diameter of M2; H_{M2}, Hole diameter of M2; D_{M3}, Diameter of M3; and H_{M3}, Hole diameter of M3

4 Characterization of A1 Surface Profile Figure of Merit

The iterative analytical model can accurately predict the size of M2 and M3 mirrors, and the geometrical photon collection area. The model is applied to different combinations of A1 profiles and entrance pupil diameters (EPDs) to determine suitable A1 surface profiles which minimizes the M2–M3 mirror sizes while satisfying the science requirement for collecting area. An alternative to forming the primary mirror from a flat membrane is to utilize several preformed slices of membranes (gores) that are stitched together to create the desired surface profile. L'Garde Inc.'s finite-element analyzer for inflatable membranes (FAIM) code provided surface profile data for quasiparabolic shaped reflectors formed from gores.[7] A 1-m monolithic membrane A1 prototype was measured with Nikon APDIS laser radar and the measured surface profile was shown to be in close accordance with the surface predicted by FAIM code.[14] The performance of L'Garde quasiparabola was compared with the case of an ideal parabola and Hencky surface. The results are shown in Fig. 6.

Although the L'Garde quasiparabola profile results in smaller M2 and M3 mirror sizes compared to the Hencky surface, they are still larger than those resulting from an ideal parabolic shape. To reduce the required diameter of M2 and M3 further system optimization is required.

Let P1 be a quasiparabolic reflector profile with base radius of curvature of 50 m at nominal pressure. P1 is decomposed to result in a best fit parabola and the residual W-curve is shown in Fig. 7. The W-curve is fit to an eighth-order polynomial and a transverse ray analysis is performed to identify the individual contribution of aspheric coefficients to the overall aberration induced by P1. Total aberration induced by P1 is equal to the combination of defocus (w_{020}) , aberration induced by fourth-order term of W-curve (w_{040}) , and aberration induced by the sixth-order term of the W-curve (w_{060}) as shown

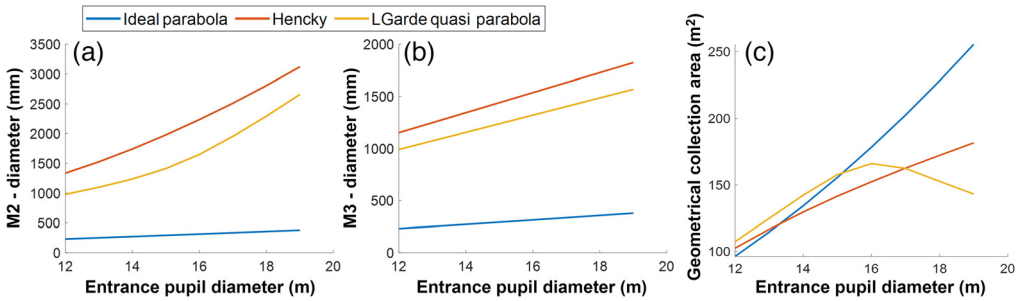

Fig. 6 Comparison between the (a) M2 mirror diameter, (b) M3 mirror diameter, and (c) Geometrical collection area of ideal parabola, Hencky, and L'Garde quasiparabola for $0 = 50$ m and $\theta = +/-0.5$ deg case.

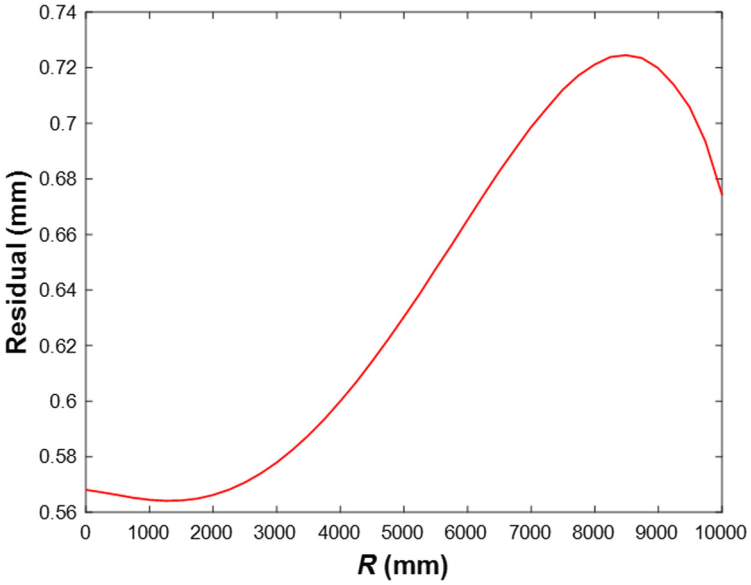

Fig. 7 *W*-curve: L'Garde near-parabola data of A1 profile is fit to an ideal parabola with base radius of 50,033.53 mm and the residual error is plotted as a function of radial distance from the A1 optical axis. (Note: This radial plot only shows the half of the "*W*" shaped *W*-curve.)

$$\varepsilon_y = -2 \times f/\# \times (2w_{020}\rho^2 + 4w_{040}\rho^4 + 6w_{060}\rho^6). \tag{7}$$

The eighth-order term is neglected as its contribution to the overall aberration is small compared to the other terms.

The transverse ray analysis yields values of, $\varepsilon_y = 671.3$ mm, $w_{040} = 10.4$ mm, $w_{060} = 12.9$ mm, and $df/\# = 1.6$. Substitution into Eq. (7) then yields

$$w_{020} = 164.4 \text{ mm}.$$

Defocus affects the location of mirrors and can be accounted for during the design process. The spherical aberration terms w_{040} and w_{060} affect the size of M2–M3 corrector mirror sizes. Reduction in the contribution of these two terms results in smaller mirrors. A scaling factor is applied to A4 and A6 aspheric terms to demonstrate its effect on M2 and M3 sizes (Table 4).

Such scaling factors can be realized by adjusting the pressure within the reflector. L'Garde data for quasiparabolic profiles with $R_1 = 50$ m, $D_1 = 20$ m at $\pm 10\%$, $\pm 20\%$, and $\pm 30\%$ of nominal pressure were analyzed to see if any of these are a close match to the profiles predicted in Table 4. Nominal pressure is the pressure required to produce a wrinkle free A1 surface of a given radius of curvature.[7] The profile at 20% lower than nominal pressure results in a M2 diameter of 500 mm and is close to the profile calculated using a scaling factor of 0.1. However,

Table 4 Variation of M2 diameter as a function of scaling factor applied to the L'Garde quasiparabola A4 and A6 aspheric coefficients of the *W*-curve.

Scaling factor	M2 diameter (mm)	Peak to valley error w.r.t. best fit parabola (mm)
1	1322	13.53
0.5	592	6.9
0.1	456	1.6
0.01	370	0.4

20% lower than nominal pressure is not sufficient to prevent wrinkles in the membranes. Therefore, a conservative scaling factor of 0.15, corresponding to a pressure yielding a wrinkle free surface, is adopted.

5 Inflatable Optical Telescope Design Solution Space

The updated definition of the A1 sag profile is used as input to the iterative analytical model and the resultant output is used to develop corresponding ZEMAX models. The next step involves numerical evaluation of the performance of these A1 profiles over the entire FOV. The terahertz heterodyne detectors are single pixel elements with a given beam width based on the observation wavelength. The goal is to efficiently couple the photons collected by the telescope into the heterodyne receivers over all the observation bands. The OASIS receiver band wavelength definitions are listed in Table 5.

The effective collection area is defined as the product of geometrical photon collection area and the area-averaged SIR and is a function of the coupling efficiency from the telescope optics to the beam expected by the heterodyne receivers ($F/16$ for OASIS). The SIR can be approximated as[15]

$$\mathrm{SIR} = e^{-\left(2\pi\frac{\sigma}{\lambda}\right)^2}, \tag{8}$$

where σ is root mean square (RMS) wavefront error as designed. Since the design accommodates FOV of ± 0.05 deg, σ averaged over FOV is used for Eq. (8). Under the assumption of σ quadratically increasing over the FOV

$$\sigma(r) = (\sigma_{\text{off-axis}} - \sigma_{\text{on-axis}})r^2 + \sigma_{\text{on-axis}}, \tag{9}$$

where r is the normalized field FOV, $\sigma_{\text{on-axis}}$ is the RMS wavefront error at FOV = 0 deg, and $\sigma_{\text{off-axis}}$ is the RMS wavefront error at FOV = 0.05 deg. Area-averaged SIR is calculated as

$$\mathrm{SIR}(r) = 2\int_0^1 re^{-\left(2\pi\frac{(\sigma_{\text{off-axis}}-\sigma_{\text{on-axis}})r^2+\sigma_{\text{on-axis}}}{\lambda}\right)^2}\mathrm{d}r. \tag{10}$$

The effective photon collection area, EA, of the system is then calculated as

$$\mathrm{EA}(r) = 2\times A_g\int_0^1 re^{-\left(2\pi\frac{(\sigma_{\text{off-axis}}-\sigma_{\text{on-axis}})r^2+\sigma_{\text{on-axis}}}{\lambda}\right)^2}\mathrm{d}r, \tag{11}$$

where A_g is the geometrical photon collection area.

Figure 8 shows contour plots of the resulting solutions space over all the four observation bands. The effective photon collection area, along with the diameters of M2 and M3, as a function of reflector radius of curvature (R1) and effective pupil diameter (EPD). The effective areas of bands 1, 2, and 3, are similar to each other, since the wavelength is much longer than the as-design optical path difference of wavefront error. Whereas the band 4 contour plots suffers from the decreased coupling efficiency due to the shorter wavelength.

Table 5 OASIS receiver bands.

OASIS receiver band	Wavelength
1	660–520 μm
2	272–136 μm
3	120–103 μm
4	63 μm

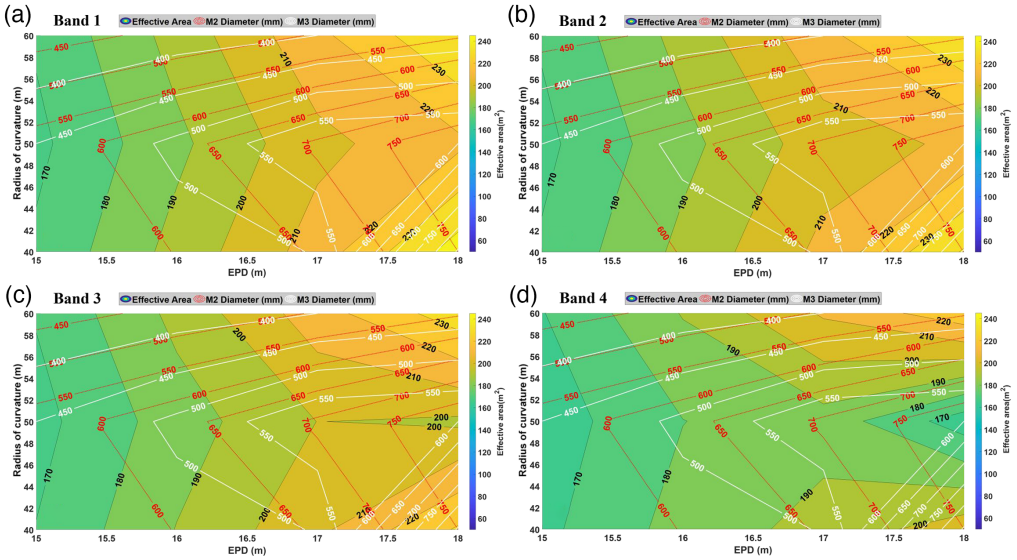

Fig. 8 (a) to (d) Inflatable optical design solution space contour plots of as designed models over the four OASIS observation bands. Effective photon collection area and diameters of M2 and M3 mirrors are plotted as a function of A1 radius of curvature and EPD.

Table 6 Baseline design parameters and the OASIS optical performance sensitivity analysis parameters.

Parameter	Value	
R_1	[40 m, 50 m, 60 m]	
D_1	[15 m, 16 m, 17 m, 18 m]	
d_{2-3}	0.7 m	
d_{IF}	100 mm	
Θ	± 0.05 deg	
A1	Decenter $X = 0.5$ mm	Tilt $X = 0.001$ deg
	Decenter $Y = 0.5$ mm	Tilt $Y = 0.001$ deg
	Decenter $Z = 0.5$ mm	Tilt $Z = 0$ deg
M2	Decenter $X = 0.1$ mm	Tilt $X = 0.001$ deg
	Decenter $Y = 0.1$ mm	Tilt $Y = 0.001$ deg
	Decenter $Z = 0.5$ mm	Tilt $Z = 0$ deg
M3	Decenter $X = 0.1$ mm	Tilt $X = 0.001$ deg
	Decenter $Y = 0.1$ mm	Tilt $Y = 0.001$ deg
	Decenter $Z = 0.5$ mm	Tilt $Z = 0$ deg

As a test of design robustness A1, M2, and M3 are individually perturbed by introducing decenter in X, Y, and Z directions and tilt about X and Y axes with values tabulated in Table 6. The system RMS wavefront error is then estimated by the root sum squares (RSS) rule of the wavefront errors of individual optical components under perturbations. The system RMS wavefront error (σ_{sys}) with respect to decenter in X, Y, and Z directions, tilt about X and Y axes of individual optical elements is given as

$$\sigma_{\text{sys}} = \sqrt{\sigma_{M1}^2 + \sigma_{M2}^2 + \sigma_{M3}^2 + \sigma_{\text{Baseline}}^2}, \tag{12}$$

where the RMS wavefront error of each individual optical elements is

$$\sigma_{\text{element}} = \sqrt{\sigma_{\text{Dec\_}x}^2 + \sigma_{\text{Dec\_}y}^2 + \sigma_{\text{Dec\_}z}^2 + \sigma_{\text{Tilt\_}x}^2 + \sigma_{\text{Tilt\_}y}^2}, \tag{13}$$

σ_{sys} is substituted in Eq. (11) and the results are shown in Fig. 8.

The contour plots show that the effective collecting area decreases due to wave front aberrations and hence the system performance degrades as the wavelength gets shorter. Tolerancing helps in determining the sensitivity of different bands to the overall system RMS wavefront error due to the perturbations of the individual optical elements. Figure 9 shows that bands 1 and 2 are less susceptible due to their longer wavelengths. After tolerancing, Band 4 shows significant degradation in the effective photon collection area. Depending on the importance of each band (e.g., concept of operations, quality and number of astronomical targets, integration time), the solution space can be recalculated using a weighing factor. The combination of A1 radii of curvatures and EPDs that would satisfy the science goals (effective collection area) and is within system architecture constraints (M2–M3 mirror sizes) can be then identified by comparing these weighted solution space contour plots. The systematic optimization flow involved in the parametric design space search resulting in solution space contour plots are presented in Fig. 10.

As an example of design optimization utilizing Fig. 9, let us assume that due to the requirement on the maximum mass of inflatant and the rate of change of surface profile with respect to pressure, a radius of curvature of 50 m is selected for A1. The EPD range can be chosen based on the required geometric collection area for the different bands as dictated by the science goals. For this example, 15 to 18 m EPD range is chosen to illustrate the application of solution space contour plots. The corresponding data from the contour plots [Figs. 9(a)–9(d)] for $R_1 = 50$ m are listed in Table 7.

Considering the maximum effective photon collection area for each band and ignoring the constraint on mirror diameter, band 1 has a peak at 17 m EPD, band 2 at 18 m, band 3 at 16 m, and band 4 at 15 m. From Table 7, an A1 with EPD of 16 m for $R_1 = 50$ m is the best choice as it still delivers close to maximum possible EAs at bands 1, 2, and 4. But if achieving the smallest possible mirror diameter has higher priority than the maximum possible EA, EPD of 15 m for $R_1 = 50$ m turns out to be the best option. Thus, plots of the type shown in Fig. 9 help in

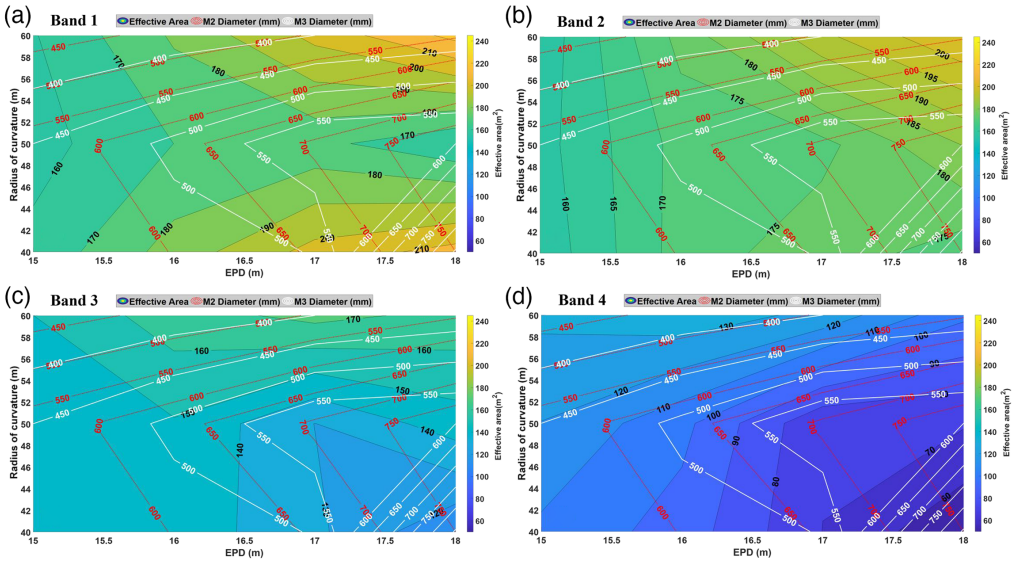

Fig. 9 (a) to (d) Inflatable optical design solution space contour plots post tolerancing over the four OASIS observation bands. Effective photon collection area using Eq. (11) and diameters of M2 and M3 mirrors are plotted as a function of A1 radius of curvature R_1 and EPD.

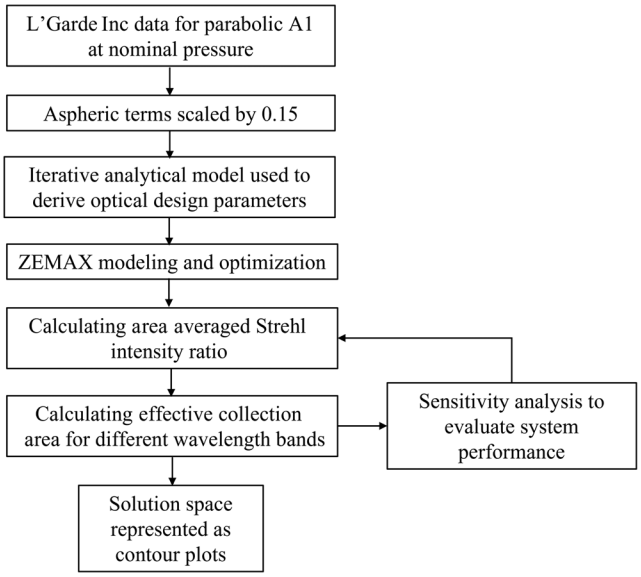

Fig. 10 OASIS parametric design space search process and inflatable optical design optimization workflow.

Table 7 Effective area and mirror diameters for $R_1 = 50$ m.

EPD (m)	Effective area (m^2)				Mirror diameter (mm)	
	Band 1	Band 2	Band 3	Band 4	M2	M3
15	156	158	147	119	574	450
16	170	171	149	103	634	510
17	173	173	129	71	708	590
18	161	185	145	71	792	600

efficiently navigating the multivariable dependencies of the design space and in identifying the most suitable A1 profile.

6 FOV Scanner Design

An FOV of ± 0.05 deg (3 arcmin) is part of the OASIS design specifications in Table 1. This is achieved by scanning the intermediate image with a tip–tilt mirror. The stop is placed at A1 in the OASIS design. A field lens made of high resistivity float zone (HRFZ) silicon is placed at the intermediate focal plane to minimize the size of the scanning mirror and to avoid vignetting during scanning. Absorption loss of HRFZ Si could be a cause of concern. But since the central thickness of the field lens is sufficiently thin (2 mm), the maximum absorption loss is at most 15%, which occurs in band 4 (Fig. 11). Reflection loss is mitigated by using the right combination and thickness of AR coating material such as Parylene.[16]

The optical layout of the scanning mechanism is shown in Fig. 12(a). The tip-tilt mirror M4 scans the intermediate image and then it is reimaged by an ellipsoidal mirror M5 to achieve the $F/16$ system as per the OASIS design specification in Table 1.

If the absorption loss of 15% at band 4 needs to be eliminated, the field lens can be replaced with a pair of mirrors as shown in Fig. 12(b). The mirror pair is rigidly connected to the tip/tilt M4 and shares the same axis about which they are rotated. In addition to the reduced loss, this configuration can also support a wider FOV of ± 0.1 deg. But in this configuration, M4 and field

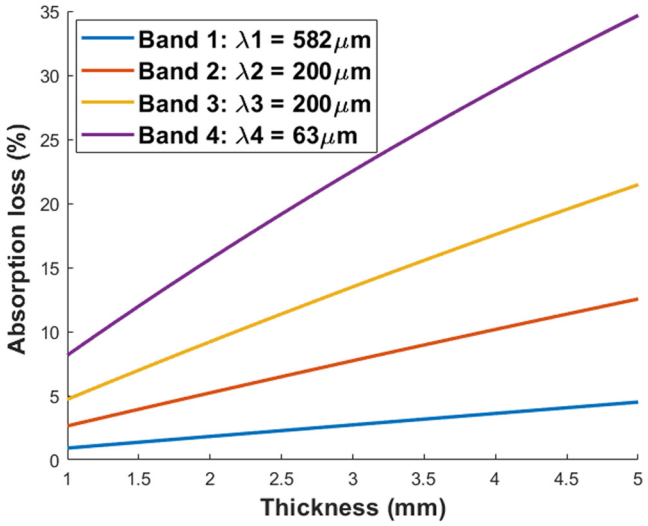

Fig. 11 Absorption loss of HRFZ Si as a function of central thickness of lens.

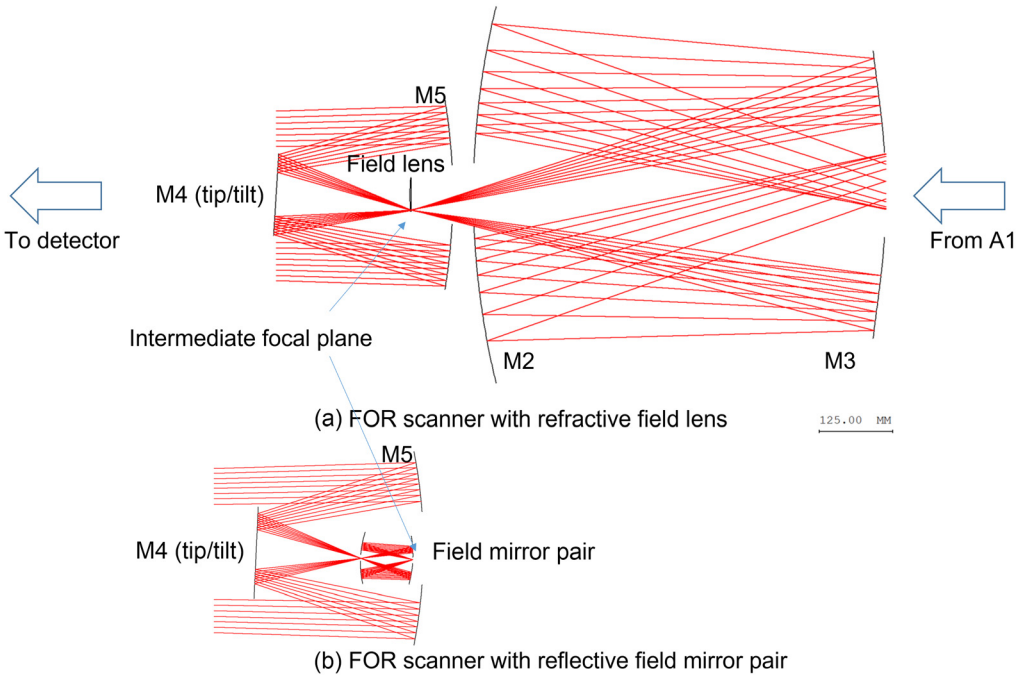

Fig. 12 OASIS FOV scanner layout with (a) HRFZ Si field lens, and (b) mirror pair (RFL1 and RFL2) replacing the field lens.

mirror pair needs to be connected and moved as one to achieve FOV scanning. Due to the increased complexity and added torque requirement on the tip/tilt mechanism, the field lens configuration is preferred.

7 MidEx Class 14-m Diameter OASIS Optical Design

7.1 *Optical Design*

Driven by the heritage of large inflatable mirror[17] and system architecture constraints,[9] the diameter of A1 was selected to be 14 m for the NASA MidEx proposal.[2] The methodologies detailed

Table 8 ZEMAX modeling results for different A1 radii of curvatures.

Radius of curvature (m)	M2 radius (mm)	M2 hole radius (mm)	M3 radius (mm)	M3 hole radius (mm)	M2–M3 distance (mm)	Geometric collection area (m^2)
40	240	50	216	50	700	142.77
50	265	50	195	65	700	126.93
60	241	50	170	75	700	100.62

in previous sections are used to redesign and optimize the corrector module, FOV scanner, and calculate the effective collection area for all the bands.

L'Garde Inc provided new data for an A1 diameter of 14 m and radius of curvature (RoC) = [40, 50, and 60 m]. The data were fit to an eighth-order polynomial and the aspheric coefficients scaled by 0.15 to produce the new A1 surface profiles. The iterative analytical model was used to design the corrector module (M2 to M3). Table 8 shows the preliminary modeling results by ray-tracing software (ZEMAX) for all the three radii of curvatures. The RoC of 40 m provides the largest geometric photon collection area with the smallest mirror dimensions.

The FOV scanning system shown in Fig. 12 was redesigned to be compatible with a commercially available hexapod (M4) H-811 from PI.[18] To prevent vignetting due to the hexapod and considering mounting constraints, M4 is mounted 45-deg off-axis. M5–M6 mirror pairs are used for further correction and to achieve $f/16$ system. Three flat mirrors, M7–M9 are used for folding the beam inside the packaging volume. Figures 13 and 14 show the MidEx Class OASIS optical design using 14-m diameter inflatable primary antenna and the spot diagrams showing diffraction-limited optical performance at $\lambda = 111$ μm (band 3).

A sensitivity analysis was performed, and effective collecting areas calculated as described in Sec. 5. Table 9 provides the effective photon collecting area derived using Eq. (11), along with the aperture efficiency, which is the ratio between the effective collection area (EA) and the geometrical membrane area (A_g).

7.2 *OASIS End-to-End Optics Loss Budget*

OASIS employs terahertz heterodyne receivers that require dichroics, beam splitters, and reimaging optics to couple the beam from the intermediate focal point to the focal plane mixers. These components reside in the receiver module (Fig. 2). A block diagram of the OASIS back-end receiver architecture is shown in Fig. 15.

Estimates for the absorption and scattering losses associated with A1, the corrector module, and receiver optics are listed in Table 10. These values are included in determining the end-to-end transfer efficiency (ε_T) and EA of the system. The results are summarized in Table 10. The aperture efficiency in Table 8 was used to estimate the effective photon collection area while considering all the optical components depicted in Figs. 13 and 15. Our analysis indicates a 14-m diameter OASIS meets mission science requirements with margin.

7.3 *Resolution of A1 Pressure Control Unit*

Since the A1 surface profile, and location of intermediate focal plane of A1–M2–M3 is a function of A1 pressure, the resolution of the pressure control unit becomes a critical parameter to match telescope beam waist at the location of heterodyne receivers. Data from L'Garde Inc for $D = 14$ m, $R = 40$ m at nominal, 10% higher, and 10% lower than nominal pressure is analyzed to determine the rate of change of base radius of curvature with respect to change of pressure. For this configuration, numerical simulation shows $dr/dp = 1.72$ mm/mPa. Considering a resolution of 0.1% of nominal pressure

$$\mathrm{dp} = 0.1\% \text{ of } P = 0.1\% \text{ of } 4.37 \text{ Pa} \approx 5 \text{ mPa}, \quad \therefore dr = 8.6 \text{ mm}.$$

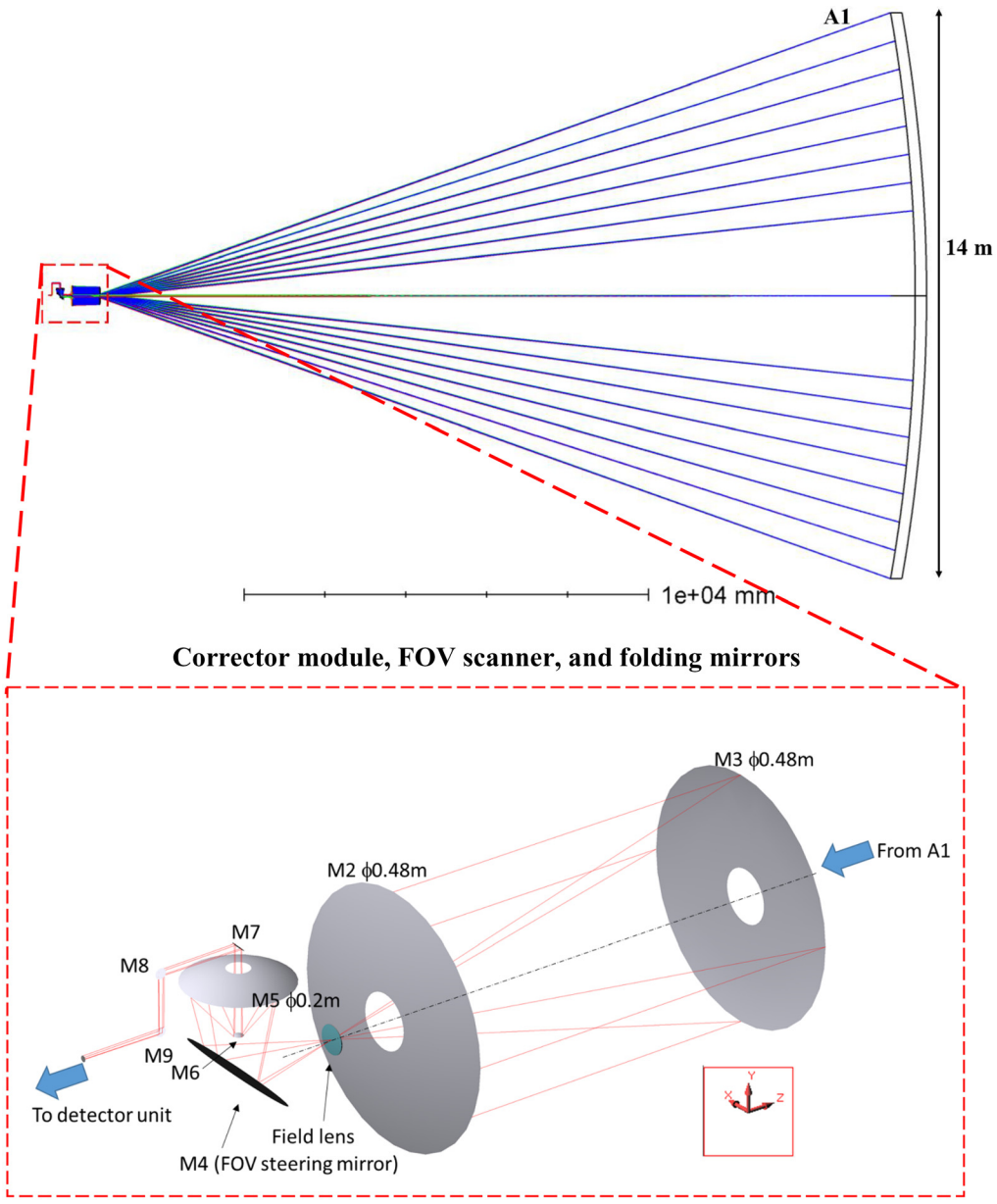

Fig. 13 Ray-trace model showing the MidEx Class OASIS optical design including the corrector module, field lens, FOV scanner, and folding mirrors for 14-m diameter primary antenna A1.

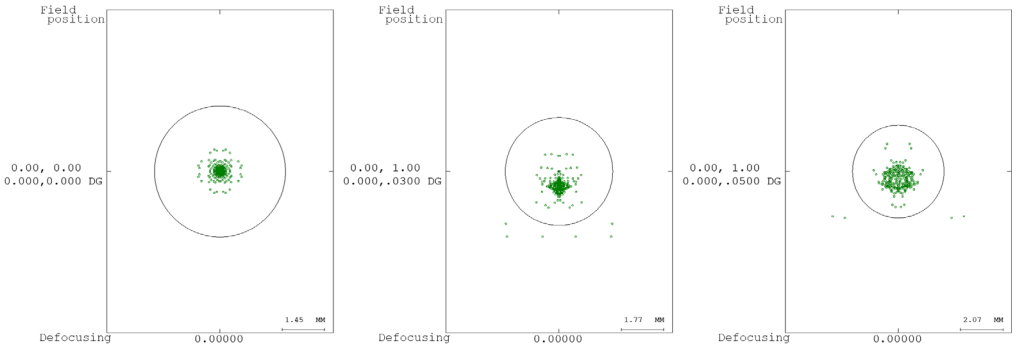

Fig. 14 MidEx Class 14-m-diameter OASIS spot diagram showing diffraction limited performance at 0 deg, 0.03 deg, and 0.05 deg FOV for $\lambda = 111$ μm (band 3).

Table 9 Effective photon collection area of the MidEx class 14-m diameter OASIS.

Band	λ (μm)	Effective collection area (m^2)	Membrane area (m^2)	Aperture efficiency
1	582	142	154	0.922
2	200	140	154	0.909
3	111	130	154	0.844
4	63	108	154	0.701

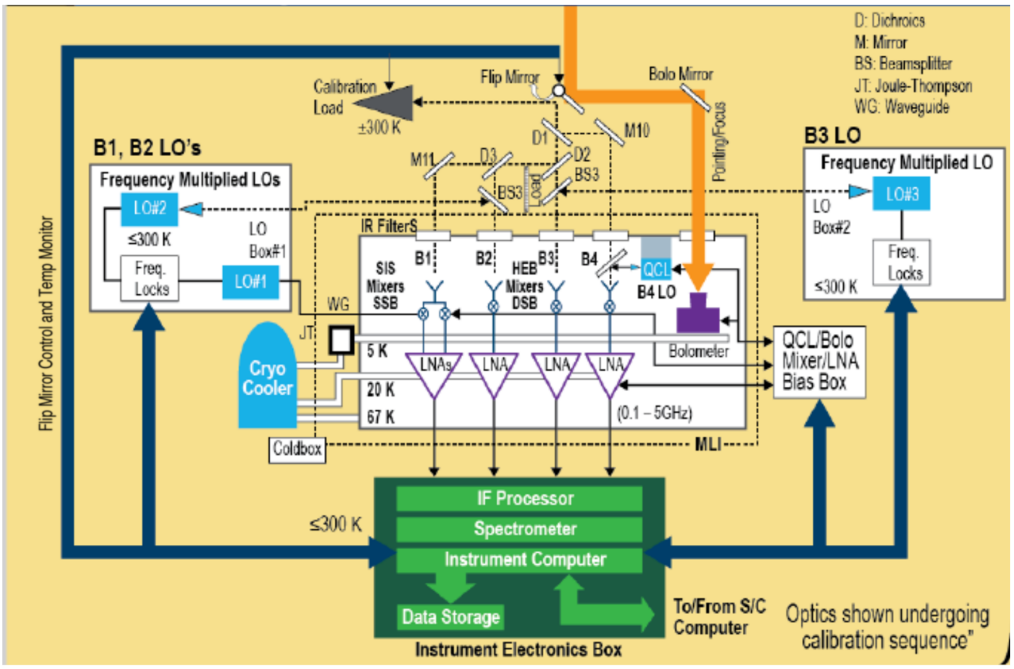

Fig. 15 Block diagram of OASIS receiver architecture.

The current design can accommodate dr (displacement of A1 along Z-axis) of 0.5 mm (Table 6). A maximum change of $dr = 2$ mm can be compensated for by using the M4 hexapod. Thus, a pressure control unit with a resolution of 1 mPa is required to maintain optimum system performance. If actuators with a travel ± 1.65 mm are incorporated into the boom design, then a resolution of 5 mPa will suffice. Long exposure of the reflector to solar UV could affect the uniformity of the polymer. However, by proper choice of coatings, deformation effects can be minimized and brought into a range that can be mitigated by the pressure control system and/or the boom actuators.[19]

8 Discussion

Starting with analytically or numerically derived surface profiles, this work has shown it is possible to realize high performance telescopes with large, inflated apertures. The next challenge from the optical design viewpoint is the compensation for thermal deformation (or unforeseen aberrations) in A1 by implementing adaptive optics (AO). AO is not required for OASIS but may prove necessary for future telescopes with inflated primaries operating at shorter wavelengths. AO is widely used on ground-based telescopes to compensate for rapid variations in the refractive index of the Earth's atmosphere due to turbulence. The changes in surface figure expected in space based inflated optics due to thermal effects will occur over minutes or hours, reducing the complexity of and demand on the AO system. In addition, the shape of A1 can be controlled by

Table 10 OASIS optics loss budget.

Module	Element	Type	Material	Loss	Band 1	Band 2	Band 3	Band 4
A1	C1	Canopy	Transparent Kapton	0.02	0.02	0.02	0.02	0.02
	A1	Reflector	Aluminized Kapton	0.01	0.01	0.01	0.01	0.01
Corrector	M2	Asphere	Aluminum	0.01	0.01	0.01	0.01	0.01
	M3	Asphere	Aluminum	0.01	0.01	0.01	0.01	0.01
	FL	Field lens	Si	0.02	0.02	0.02	0.02	0.02
	M4	Flat: FOV scanner	Aluminum	0.01	0.01	0.01	0.01	0.01
	M5	Asphere	Aluminum	0.01	0.01	0.01	0.01	0.01
	M6	Asphere	Aluminum	0.01	0.01	0.01	0.01	0.01
	M7	Flat	Aluminum	0.01	0.01	0.01	0.01	0.01
	M8	Flat	Aluminum	0.01	0.01	0.01	0.01	0.01
	M9	Flat	Aluminum	0.01	0.01	0.01	0.01	0.01
Receiver	D1	Frequency diplexer	Mesh	0.05	0.05	0.05	0.05	0.05
	D2	Frequency diplexer	Mesh	0.05	0.05	0.05	0.05	—
	D3	Frequency diplexer	Mesh	0.05	0.05	0.05	—	—
	B2	Beam splitter	Mylar	0.01	—	0.01	—	—
	B3	Beam splitter	Mylar	0.01	—	—	0.01	
	B4	Beam splitter	Mylar	0.01	—	—	—	0.01
	F1	IR filter	Mesh	0.02	0.02	—	—	—
	F2	IR filter	Mesh	0.02	—	0.02	—	—
	F3	IR filter	Mesh	0.02	—	—	0.02	—
	F4	IR filter	Mesh	0.02	—	—	—	0.02
	M10	Flat	Aluminum	0.01	—	—	—	0.01
	M11	Elliptical	Aluminum	0.02	0.02	—	—	—
		Transmission efficiency			0.68	0.69	0.74	0.78
		Aperture efficiency			0.922	0.909	0.844	0.701
		Transfer efficiency			0.63	0.63	0.62	0.54
		Membrane area			154	154	154	154
		Effective collection area			96.6	96.6	96.0	84.2
		Requirement (10× Herschel)			56	56	56	56
		Margin			42%	42%	42%	34%

precisely modulating the pressure. This can be used in conjunction with the AO to correct for thermal variations in A1.

9 Conclusion

The OASIS is an inflatable terahertz space telescope with a 14-m diameter primary reflector realized with a pressurized, metalized polymer membrane. We established a systematic optical

design process for optimizing the performance of space telescopes employing inflatable primary reflectors of various sizes. The formulation enables a comparison of inflatable primary reflector geometries, such as Hencky reflectors formed from a monolithic flat gore, as well as quasiparabolic reflectors formed from segmented and sealed gores. The comprehensive design process identified a baseline design for OASIS satisfying all major requirements, such as effective photon collection area and size of corrector optics, as well as tolerancing requirements. Thus, this work provides a roadmap for addressing the unique challenges associated with realizing the great potential of large inflatable optics for space applications.

References

1. W. Martin et al., "Hydrothermal vents and the origin of life," *Nat. Rev. Microbiol.* **6**(11), 805–814 (2008).
2. 2021 Medium Explorer (MIDEX) – Solicitation No. NNH21ZDA018O.
3. C. Walker et al., "Orbiting Astronomical Satellite for Investigating Stellar Systems (OASIS) following the water trail from the interstellar medium to oceans," *Proc. SPIE* **11820**, 118200O (2021).
4. G. L. Pilbratt et al., "Herschel space observatory," *Astron. Astrophys.* **518**, 7–8 (2010).
5. H. Hencky, "Uber den Spannungszustand in kreisrunden Platten," *Z. Math. Phys.* **63**, 311–317 (1915).
6. W. B. Fichter, "Some solutions for the large deflections of uniformly loaded circular membranes," NASA Technical Paper 3658 (1997).
7. A. L. Palisoc et al, "Analytical and finite element analysis tool for nonlinear membrane antenna modeling for astronomical applications," *Proc. SPIE* **11820**, 118200U (2021).
8. J. H. Burge et al., "Development of a wide-field spherical aberration corrector for the Hobby Eberly Telescope," *Proc. SPIE* **7733**, 77331J (2010).
9. J. W. Arenberg et al, "OASIS architecture: key features," *Proc. SPIE* **11820**, 118200S (2021).
10. J. R. G. Silva et al., "4 × 2 HEB receiver at 4.7 THz for GUSTO," *Proc. SPIE* **10708**, 107080Z (2018).
11. A. B. Meinel and M. P. Meinel, "Inflatable membrane mirrors for optical passband imagery," *Opt. Eng.* **39**, 541–550 (2000).
12. A. Offner, "A null corrector for paraboloidal mirrors," *Appl. Opt.* **2**, 153–155 (1963).
13. J. E. Greivenkamp, *Field Guide to Geometrical Optics*, SPIE, Bellingham (2004).
14. S. Sirsi et al., "Modeling and characterization of OASIS inflatable primary antenna by dual modality metrology," submitted to *Optics Express* (Manuscript ID: 464429).
15. V. N. Mahajan, "Strehl ratio for primary aberrations in terms of their aberration variance, *J. Opt. Soc. Am.* **73**, 860–861 (1983).
16. A. J. Gatesman et al., "An anti-reflection coating for silicon optics at terahertz frequencies," *IEEE Microwave Guided Wave Lett.* **10**(7), 264–266 (2000).
17. R. E. Freeland et al., "Large inflatable deployable antenna flight experiment results," *Acta Astron.* **41**(4–10), 267–277 (1997).
18. Physik Instrumente, "H-811.I2 6-axis miniature hexapod," https://www.pi-usa.us/en/products/6-axis-hexapods-parallel-positioners/h-811i2-6-axis-miniature-hexapod-700886/ (accessed 6 July 2022).
19. S. Miller and J. Dever, "Space environment exposure results from the MISSE 5 polymer film thermal control experiment on the international space station," 2009, https://ntrs.nasa.gov/citations/20120015086.

Siddhartha Sirsi is a PhD candidate in electrical engineering. He completed his MS degree in optical sciences from the University of Arizona in 2021. His main areas of research are superconducting transistors, terahertz astronomical instrumentation design, and optical design and metrology of inflatable telescopes. He is part of the Steward Observatory Radio Astronomy Lab and Large Optics and Fabrication and Testing Lab at UofA. He completed his MS degree in ECE from Arizona State University in 2014.

Yuzuru Takashima is a professor at James C. Wyant College of Optical Sciences of University of Arizona. His research focus is MEMS-based lidar for automotives and AR displays for Metaverse, as well as optical design in general, including space optics. Prior to joining the University of Arizona, he was a research staff at Stanford University where he conducted research and development of high density holographic data storage systems and nano-photonic electron beam generators. He was employed as an optical engineer at Toshiba Corporation in Japan and developed ultraprecision manufacturing process for optical components. He is a senior member of Optica and SPIE, serving as a cochair of a conference, Industrial Optical Systems and Devices (iODS). He received his BS degree in physics from Kyoto University in Japan and his MS and PhD degrees in electrical engineering from Stanford University.

Biographies of the other authors are not available.